Resident Neuroelectrochemical Interfacing Using Carbon Nanofiber Arrays

Timothy E. McKnight,*,†,‡ Anatoli V. Melechko,‡,|| Benjamin L. Fletcher,‡,|| Stephen W. Jones,†,‡ Dale K. Hensley,‡ Diana B. Peckys,‡,# Guy D. Griffin,§ Michael L. Simpson,‡,|| and M. Nance Ericson†

Monolithic Systems Development Group, Oak Ridge National Laboratory, Molecular Scale Engineering and Nanoscale Technologies Research Group, P.O. Box 2008, Oak Ridge, Tennessee 37831-6006, Advanced Biomedical Science and Technology Group, Oak Ridge National Laboratory, Materials Science and Engineering Department, University of Tennessee, and Center for Environmental Biotechnology, University of Tennessee

Received: November 8, 2005; In Final Form: June 8, 2006

Carbon nanofiber electrode architectures are used to provide for long-term, neuroelectroanalytical measurements of the dynamic processes of intercellular communication between excitable cells. Individually addressed, vertically aligned carbon nanofibers are incorporated into multielement electrode arrays upon which excitable cell matrixes of both neuronal-like derived cell lines (rat pheochromocytoma, PC-12) and primary cells (dissociated cells from embryonic rat hippocampus) are cultured over extended periods (days to weeks). Electrode arrays are characterized with respect to their response to easily oxidized neurotransmitters, including dopamine, norepinephrine, and 5-hydroxytyramide. Electroanalysis at discrete electrodes following long-term cell culture demonstrates that this platform remains responsive for the detection of easily oxidized species generated by the cultured cells. Preliminary data also suggests that quantal release of easily oxidized transmitters can be observed at nanofiber electrodes following direct culture and differentiation on the arrays for periods of at least 16 days.

Background

Neuroelectrochemical interfacing via micromanipulated micro- and nanoscale electrodes has been established as a powerful tool for unraveling the dynamic events of exocytosis, a predominant mechanism of chemical communication between neuronal cells. Since the early pioneering efforts in the Adams Laboratory with carbon paste electrodes[1], refinements to electrode geometries[2] and measurement techniques have provided enormous insight into the mechanisms,[3−6] subtleties,[7] and pharmacological responses[8,9] surrounding the processes of vesicular release of neurotransmitters from excitable cells. Several of these neurotransmitters, including dopamine, norepinephrine, and serotonin are easily oxidized at carbon electrodes, enabling their detection and quantitation using electrochemical techniques. A well-established practice is to entrain a carbon fiber electrode material within a glass capillary and micromanipulate this electrode adjacent to a cellular region of interest, thereupon using techniques such as fast scan cyclic voltammetry and constant potential amperometry to resolve the release of these easily oxidized materials from the targeted cell. Positioning of multiple elements, while arduous, has been used to resolve simultaneous events at discrete locations of a cellular matrix, providing extremely high temporal and spatial resolution of these near molecular scale events.

Recently, we have been developing resident, nanostructured electrode systems for cellular interfacing.[10−12] In contrast to the conventional use of individual, micromanipulated glass-capillary-based probes, our approach is similar to the established use of planar electrode arrays for in vitro interfacing to cellular matrixes where cells are cultured directly on the electrode array. However, incorporation of a unique electrode material, the vertically aligned carbon nanofiber (VACNF),[13−17] enables the integration of nonplanar, high aspect ratio features as the electroactive elements of the device. VACNFs are cylindrical structures synthesized by catalytic plasma enhanced chemical vapor deposition and composed of graphitized carbon of various configurations with typical diameters varying between tens to hundreds of nanometers and lengths up to 100 μm. These nonplanar features provide the ability to locate the electroactive surface of electrodes significantly (tens of micrometers) *above* the planar substrate. This enables location of the electroactive region potentially *intercellularly* within an excitable cell matrix, rather than between the cells and the underlying substrate as occurs with planar electrode structures. We hypothesized that this nonplanar aspect may provide novel approaches for electroanalytical probing techniques and particularly for the monitoring of chemical modes of communication *between* cells, such as those that occur during synaptic neural transmission. We anticipated that our electrode material, the VACNF, may behave similarly to the conventional single-element probes used for such electroanalytical measurements which are constructed of carbon microfibers encased into pulled glass-capillary sheaths. A potential advantage of our architecture, however, is that these nanofiber-based probes can be integrated into massively parallel

* To whom correspondence should be addressed. Phone: 865-574-5681. Fax: 865-576-2813. E-mail mcknightte@ornl.gov.

† Monolithic Systems Development Group, Oak Ridge National Laboratory.

‡ Molecular Scale Engineering and Nanoscale Technologies Research Group.

§ Advanced Biomedical Science and Technology Group, Oak Ridge National Laboratory.

|| Materials Science and Engineering Department, University of Tennessee.

Center for Environmental Biotechnology, University of Tennessee.

10.1021/jp056467j CCC: $33.50
Published on Web 07/19/2006 PAGE EST: 10.4

electrode arrays using the cost-effective and readily available techniques of microfabrication.[10] As such, in contrast to independently manipulating a small number of pulled capillary-based carbon probes, our platform may provide the ability to interface to an excitable cell matrix on a highly parallel basis. Further, since these probes can be synthesized on a small, planar substrate, they may be used in a mode where cells or tissue are cultured directly on the penetrant electrode array for long periods of time. This resident mode of interfacing may provide novel approaches for longer-term studies of the dynamic processes of chemical communication between excitable cells.

This study investigates the potential of nanofiber-based electrode architectures for interfacing with excitable cell matrixes. We describe the fabrication of two types of nanofiber-based electrode arrays and characterize the performance of these arrays for electroanalytical measurement of several easily oxidizable neurotransmitters. Cell culture and long-term neuronal differentiation (at least 16 days) directly on the electrode array is then demonstrated. Activity of discrete nanofiber electrodes is maintained throughout this culture period, as evidenced by both electrophysiological coupling with nicotine induced depolarization of undifferentiated cells and electroanalytical detection of easily oxidized species within the electrode probing volume following a period of cellular differentiation. Preliminary data also suggests that these systems may be used to discretely measure exocytotic events from the differentiated cell culture at individual elements of the nanostructured electrode array.

Materials and Methods

Materials. Analytes for electrochemical characterization of probe arrays were acquired from commercial sources and used as received. Ruthenium hexamine trichloride was purchased from Aldrich. Dopamine, norepinephrine, and serotonin were purchased from Sigma and used without further purification. Neurobasal/B27 medium was purchased from Life Technologies and supplemented with 25 μM glutamate and 0.5 mM glutamine. Kaighn's Modified Ham's F12 (F12-K) was purchased from ATCC premixed with 2 mM L-glutamine and 1500 mg of sodium bicarbonate and supplemented with 15% horse serum and 2.5% bovine serum (Invitrogen). PC-12 differentiation media was prepared from Kaighn's Modified Ham's F12 with 2 mM L-glutamine and 1500 mg of sodium bicarbonate by supplementing with 1% horse serum, 0.2% fetal bovine serum, 100 units/mL of penicillin/streptomycin, and 50 ng/mL nerve growth factor derived from mouse submaxillary gland (Sigma). Tyrodes solution was prepared as 10 mM HEPES, 145 mM sodium chloride, 5 mM potassium chloride, 2 mM calcium chloride, 0.7 mM magnesium chloride, and 10 mM glucose and pH adjusted to 7.35. Fibronectin was purchased as a 0.1% solution (1 mg/mL) in 500 mM NaCl and 10 mM Tris and diluted to 50, 10, and 1 μg/mL in phosphate-buffered saline (PBS, 150 mM NaCl, 10 mM phosphate, pH 7.4). Gluteraldehyde was purchased as an 8% solution from Electron Microscopy Sciences and diluted to 2% in phosphate buffered saline.

Fabrication of VACNF Electrode Arrays. Two styles of devices were investigated in this study, each incorporating arrays of VACNFs as the active elements of the device. The Type I array is a 5-mm square probe array having 10 groups of 4 individually addressed nanofibers at an intergroup spacing of approximately 400 μm. The Type II array is a 15-mm square die featuring a linear array of 40 individually addressed nanofibers at a 15-μm pitch at the center of the device. The basis of our approach to fabricate individually addressable nanofiber arrays has been previously reported in detail[10,11] and is briefly summarized here for clarity. N-type silicon wafers are first thermally oxidized with 1 μm of silicon dioxide to isolate the top levels of the device from the underlying substrate. The wafers are then metallized with 100 Å of Ti, 1000 Å of W, 100 Å of Ti, and 100 Å of Si using electron-beam physical vapor deposition at 10^{-6} Torr. Sites for fiber growth are defined photolithographically as either 500-nm diameter dots for the Type I array or 2-μm dots for the Type II array. Following development, a 30-s oxygen plasma etch is used to remove photoresist residue in developed regions. The wafer is then metallized with 500 Å of nickel catalyst for Type I arrays and 1000 Å for Type II arrays using electron-beam physical vapor deposition. Liftoff of the excess Ni outside of the regions where nanofibers are to be grown is provided by dissolving the photoresist layer with acetone, followed by brief ultrasonication and rinsing in 2-propanol. As a result, nickel catalyst films remain only in locations where nanofibers are to be grown. Fiber synthesis is conducted in a direct current plasma-enhanced chemical vapor deposition process (dc-PECVD) where catalytic decomposition of acetylene on nickel results in "tip-type" nanofibers. In this growth mode, each catalyst particle is elevated from the substrate and remains on the fiber-tip during growth. Growth is continued for a specific time period to provide fibers of desired length, 7−10 μm for this application. During this growth, the underlying metallization (Ti/W/Ti/Si) serves as the cathode for the dc plasma. Following fiber growth, electrode interconnect patterns are lithographically defined on this metallization to protect desired interconnect patterns beneath a layer of photoresist. Noninterconnect metallization is then removed from the unprotected regions with a reactive ion, refractory metal etch ($SF_6/O_2/CHF_3$). A passivation layer of ~100 nm of PECVD silicon dioxide is then coated conformally on all surfaces (interconnects, substrate, and fibers). The wafer is then spun with approximately 2−3 μm of a negative tone photoresist (SU-8, Microposit), which is then lithographically defined to provide contact pad vias at the periphery of each die. An optional second layer of SU-8 resist is then spun on at a thickness greater than the length of the nanofibers, typically 15−20 μm. In this study, the second layer of SU-8 was applied to the Type I array but not to the Type II array. Fibered regions and contact pads are cleared of this deep SU-8 layer lithographically. An oxygen inductively coupled plasma etch process is then used to remove (ash) residual SU-8 resist and to emancipate the oxide-coated nanofiber tips from SU-8 residual that can accumulate on the fiber surface during processing of the first SU-8 layer. This step also roughens the SU-8 surface and increases its hydrophilicity, promoting subsequent cellular adhesion or optional functionalization with extracellular matrix materials to further promote such attachment. Finally, a silicon dioxide reactive ion etch is used to emancipate *only the nanofiber tips* from the silicon dioxide and to open the peripheral contact pads. Alternatively, a wet etch in 6:1 HF buffered oxide etch can be used to strip *all* silicon dioxide from the nanofibers and contact pads, thereby providing a larger electroactive surface area at each nanofiber probe.

Packaging of VACNF Electrode Arrays. Wafers of VACNF electrode arrays were spun with a thick protective layer of photoresist (SPR220 CM 7.0, Microposit) and diced to provide individual die measuring either 5-mm square (Type I) or 15-mm square (Type II). Following dicing, the die were individually stripped of the protective photoresist using a 30-min soak in acetone, followed by rinsing in acetone, 2-propanol, and Nanopure water. The Type I die were attached with epoxy into

the recessed cavity of a ceramic 40-pin dual inline package (DIP, Spectrum Semiconductor) and interconnected to the DIP via aluminum wirebonds. The active electrode region of the device was then capped with a 1 mm × 4 mm block of precast poly(dimethylsiloxane) (PDMS, Sylgard 184, Dow Corning, Midland MI) approximately 3 mm tall. The DIP cavity was then heated to 65 °C and backfilled with medical grade epoxy (FDA2T, Tracon, MA) to encapsulate the wirebonds for both passivation and mechanical stability. Following epoxy cure at 65 °C for 1 h, a ring of the same epoxy was applied around the top of the potted region. A 35-mm diameter cell culture dish (Nunc Delta) with a predrilled 5-mm hole in its center was affixed to the DIP package and cured in place at 65 °C for 1 h. Prior to use, the PDMS cap covering the active region of the device was removed with forceps. The packaged device was then soaked in acetone for 30 min, followed by 95% ethanol soak for 30 min to provide sterilization of the exposed surfaces. The cell culture dish was then rinsed in triplicate with sterile, distilled water.

The Type II die were epoxy mounted onto a custom built printed circuit board (PCB) featuring 40 bonding pads and interconnects on the periphery of the PCB. Aluminum wirebonds were used to interface the PCB to the nanofiber array. A glass cylinder measuring 8 mm OD, 6 mm ID, and 4 mm tall was then attached with medical-grade epoxy (FDA2T) to the active region at the center of the device to provide fluid containment above the active nanofiber elements. The packaged Type II device was then soaked in acetone for 30 min, followed by 95% ethanol soak for 30 min to provide sterilization of the exposed surfaces. The reservoir defined by the cylinder was then rinsed in triplicate with sterile, distilled water.

Precharacterization of Nanofiber Electrodes. Techniques to precharacterize the performance of nanofiber electrodes have previously been described in detail[11] and are iterated here for clarity. The active surface area of each electrode is approximated from cyclic voltammetry by measuring the steady-state reduction current of ruthenium hexamine trichloride at various concentrations (1, 3, 5, and 10 mM in 300 mM KCl) against a Ag|AgCl (3 M KCl) reference electrode in two-wire mode.

System capacitance of each electrode is determined by cyclic voltammetry in a nonelectroactive solution (100 mM KCl) at various scan rates and linear regression analysis of the capacitance as a function of the resultant capacitive current and the voltammetric scan rate.

Electrode responses to various electroactive neurotransmitters were also pre-characterized via cyclic voltammetry and differential pulse voltammetry using 1, 3, and 5 mM concentrations of dopamine, norepinephrine, and serotonin in Tyrodes solution. These characterizations were performed both against a Ag|AgCl (3 M KCl) reference electrode and a platinum wire pseudoreference in Tyrodes solution.

Surface Treatment of Electrode Arrays. Packaged nanofiber electrode arrays were pretreated with dilute solutions of either poly-L-lysine (PLL) or fibronectin to promote cell attachment and neuronal process development. Dilute solutions of 1, 10, and 50 μg/mL fibronectin (or PLL) in PBS were applied to the chips and incubated for 60 min at 37 °C, 100% relative humidity (RH). Following incubation, these solutions were aspirated off the chip, and the chip was rinsed in triplicate in sterile water. Some array samples were then reanalyzed with ruthenium hexamine trichloride to ensure that electrode response was not eliminated due to the coating procedure.

Cell Culture. Commercially available rat hippocampal cells (BrainBits, LLC, Springfield, IL) were dissociated following manufacturer's procedures and seeded onto nanofiber array chips at approximately 200 cells/mm^2. Cells were plated in Neurobasal/B27 medium supplemented with 20 μM glutamate and 0.5 mM glutamine. One-half of the cell media was aspirated every three days and replaced with fresh media. Cultures were maintained at 37 °C, 5% CO_2, and 100% RH.

Rat pheochromocytoma cells (PC-12) were maintained in nondifferentiated culture in a Falcon T-75 flask under F12-K supplemented with 15% horse serum and 2.5% fetal bovine serum. Media was aspirated and replaced every 3 days. Cells were harvested from nondifferentiated culture by aspiration of media and trituration with 5 mL of fresh medium. Mechanical dissociation was provided via trituration through a 5-mL pipet (Costar). Cells were plated onto nanofiber array chips in nondifferentiation media and allowed to attach for 24 h at 37 deg C, 5% CO2, and 100% RH. Media was then aspirated and replaced with PC-12 differentiation media. Every three days, one-half of the media was aspirated and replaced with fresh differentiation media.

Monitoring of Attachment and Outgrowth of Neurite Processes. Cell culture on nanofiber array chips was monitored via optical microscopy using a dissection microscope (40×) and a brightfield reflection scope (Mitutoyo WF with M Plan APO 10× and 20× objectives). Post-experimental images of cultured arrays were also obtained by scanning electron microscopy (SEM). To prepare cells for SEM imaging, the cultures were aspirated of media and rinsed in triplicate with PBS. PBS was then aspirated and replaced with a solution of 2% gluteraldehyde in PBS. Cells were incubated at 37 °C for 30 min in this fixative and then rinsed in PBS and then water. Finally, the volume of water was dropwise exchanged with methanol over a period of approximately 10 min. The methanol was then aspirated, and the samples were allowed to dry at room temperature. Imaging was then conducted in a Hitachi 4700S scanning electron microscope at 1-kV acceleration voltage using its lower detector mode, where the detector is positioned to collect secondary electrons in a wide energy range and is thus less sensitive to surface charging. This feature allows imaging cells without the necessity of sputtering a metal coating.

Activity Recording. Cultured VACNF arrays were aspirated of media and replenished with 37 °C Tyrodes solution. The array was placed in a Faraday cage with individual nanofiber electrodes connected as the working electrode of a two-wire electrochemical analysis system. A platinum pseudoreference/counterwire was flame sterilized and placed into the Tyrodes solution with care so as to not mechanically interact with the attached cell monolayer. Ag|AgCl wire was also used in short experiments where long-term cell viability was not required. Activity at the nanofiber electrode was monitored by cyclic voltammetry, typically by scanning between −0.8 and 0.8 V vs Pt (pseudo) at scan rates from 500 to 10 V/s. Constant potential amperometry was also conducted by applying potentials sufficient to oxidize dopamine and norepinephrine (0.80 vs Pt pseudo) at the nanofiber electrode and monitoring oxidation current over a period of typically 30 s to several minutes. In many experiments, the applied potential to the working electrode was sufficient to induce excitable activity in the neighboring cell matrix. Cell stimulation was also applied in some experiments by either replacement of the Tyrodes solution with an equal volume of Tyrodes with 1 mM nicotine or by application of a secretogogue, K^+, to the solution via pipet or pulled capillary.

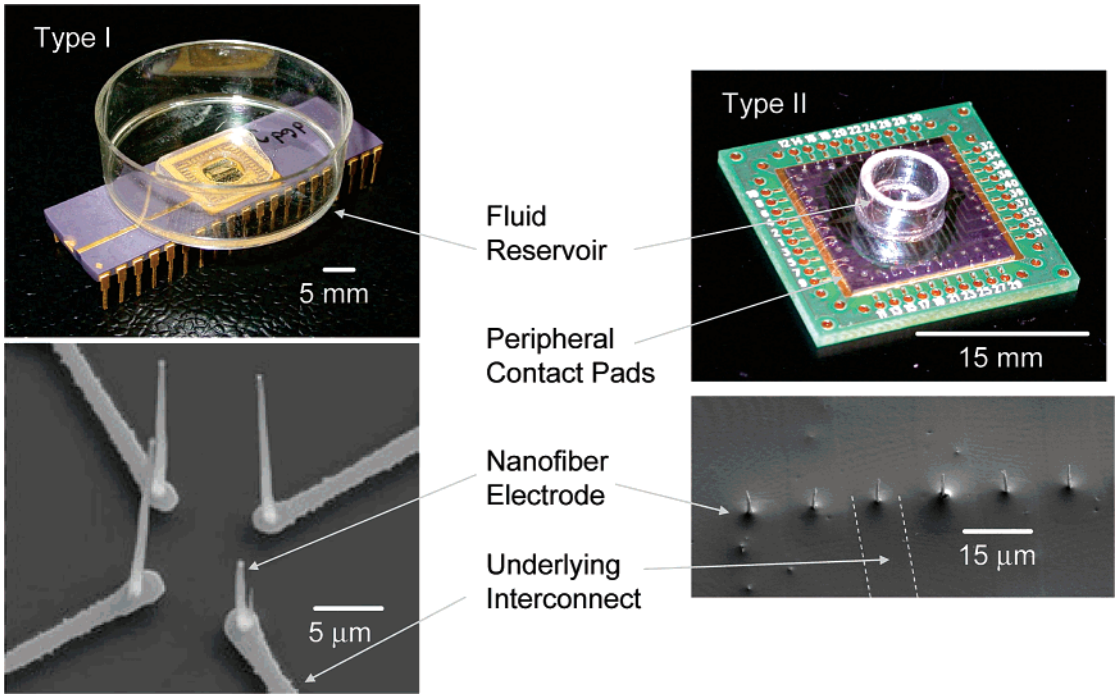

Figure 1. The Type I nanofiber array, shown at left packaged in a 40-pin dual inline package and attached to a 35-mm cell culture dish. Each array features 40 individually addressed nanofiber electrodes configured as 10 groups of 4. At the bottom: a group of 4 electrodes is shown prior to subsequent deposition of PECVD SiO_2 and SU-8 epoxy passivation layers. The Type II nanofiber array, shown at right, features 40 individually addressed nanofiber electrodes. These emerge above a 3−5-μm thick layer of UV-cross-linked photoresist in a fluidic reservoir at the center of a 15-mm square die. Individual nanofiber electrodes are spaced at 15 μm intervals.

Results and Discussion

Fabrication of Nanofiber Electrode Arrays. Photographs of Type I and Type II nanofiber array types are shown in Figure 1. The devices employed in this study featured carbon nanofiber electrodes deterministically grown from photolithographically defined nickel catalyst films. Type I electrode arrays were fabricated using projection lithography for the nickel catalyst and metal interconnect definition steps. Projection lithography with 5× reduction enabled the patterning of nickel disks down to approximately a 400-nm diameter. Such disks produced singular nanoparticles and therefore singular nanofibers during nanofiber synthesis. These nanofibers typically measured 100 nm in diameter and approximately 10 μm in length, with the latter depending on the specific growth time, i.e., the duration of the plasma. Projection lithographic definition of the interconnect pattern provided discretely addressed nanofibers that could be spaced as close as 2 μm while still providing individual electrical addressability.

Type II electrodes were fabricated exclusively with contact photolithography. As such, nickel catalyst disks and interconnect patterns could not be defined with the same resolution as that provided by i-line projection photolithography with reduction, but they can me made at much lower cost. Typically, contact photolithographically defined catalyst disks measured approximately 1−2 μm in diameter. These larger catalyst disks tended to break up during the initial phases of nanofiber growth, and the nanoparticles that formed from each disk varied in size significantly. Growth/etch conditions can be chosen such that only the largest particles survive during growth, thereby generating a single free-standing nanofiber. Additionally, we have observed that for a small group of closely spaced nanofibers, there is a difference in the growth rates that is likely caused by change in the local environment around the nanofiber group (i.e., e-field, ion flux, etc). This appears to increase the growth rate of the highest fiber, such that one fiber often grows taller than the others within the local grouping of fibers. As such, these bunched groups of fibers would often still feature 100-nm diameter tips but would have a more conical aspect than a singular, projection defined nanofiber, due to bunching of the multiple fibers down the length of the group. The interconnect pattern provided by contact lithography allowed individual addressability of these groups at a 15-μm pitch.

Device Packaging. Packaging of the Type I device required "capping" the device active region during epoxy-based passivation, or *potting*, of the peripheral wirebonds. This procedure necessitated the use of a recessed well, or channel, in which the nanofiber electrodes could be sequestered and protected during the potting step. The channel region was capped with precast PDMS to prevent the epoxy potting material from flowing onto the underlying nanofiber electrodes while passivating all other regions of the device, including the wirebonds. While effective, this approach generated an architecture that proved difficult to use for a variety of reasons. The limited size of the channel structure proved difficult to wet, often requiring the use of wetting agents, such as ethanol or sodium dodecyl sulfate (SDS), prior to analyte characterization. As the presence of these agents can be problematic with respect to subsequent cell culture, this wetting problem often impacted the ability to seed the devices uniformly with cells.

The Type II devices were overall much more convenient to use in all experiments. The much larger die size (15 mm square vs the 5 mm square Type I) allowed the attachment of reservoirs to the active region of the device without necessitating subsequent potting of the peripheral wirebonds. The entire array and its mating printed circuit board could be placed into a 35-mm cell culture dish for convenient handling during subsequent cell culturing activities.

Characterization of Nanofiber Electrode Response. Previously, the performance of individually addressed, vertically aligned, carbon nanofibers has been documented using a variety

of quasi-reversible analytes including ruthenium hexamine trichloride, iridium hexachloroiridate, and potassium ferrocyanide.[11] $Ru(NH_3)_6Cl_3$ is a quasireversible outer sphere redox species that has been demonstrated to not significantly adsorb onto nanofiber electrodes. As such, it is used routinely in our laboratory for precharacterization of electrode performance, including electroactive surface area, specific capacitance, and electron-transfer kinetics of nanofiber electrodes. Surface area may be approximated from the steady-state reduction current of $Ru(NH_3)_6^{3+}$ by assuming a semihemispherical electrode geometry and employing the expression for semihemispherical microelectrodes

$$r = \frac{i_{ss}}{2\pi nFDC}$$

where i_{ss} is the measured steady-state reduction current, $n = 1$ (for a 1-electron-transfer reaction), F is Faraday's constant, D is the diffusion coefficient of $Ru(NH_3)_6^{+3}$ in 100 mM KCl, and C is the concentration (0.001−0.010 M). While this approximation does not account for the cylindrical aspect of nanofiber electrodes and rather provides the radius of an assumed semihemispherical geometry, it does provide a fair approximation of the equivalent active surface area. In this effort, electrode arrays were constructed with fibers ranging from approximately 3−10 μm tall with an electroactive surface area ranging from approximately 0.5−10 μm^2. More accurate determination of the electrode geometry, and therefore its true radius and length, can be provided by SEM, using low acceleration voltages (0.5−2 kV) in order to minimize charging effects on the passivated surface of the device. Typical electrode radii ranged from approximately 80−200 nm for the Type I device and 100−400 nm for the Type II array.

In addition to precharacterization with quasireversible, outer sphere analytes, the response of nanofibers to several easily oxidizable monoamine neurotransmitters, specifically dopamine, norepinephrine, and 5-hydroxytryptamine (5-HT, serotonin), was also evaluated. Because of the similar oxidation potentials of these neurotransmitters, differential pulse voltammetry was used to better discriminate the oxidation potential of each material. Solutions of 3 mM dopamine, norepinephrine, and 5-HT were prepared in Tyrodes solution, and differential pulse voltammetry was performed vs a platinum pseudoreference electrode (0.28 V open circuit potential vs Ag|AgCl (3 M KCl) in Tyrodes). The pulse amplitude and pulse period for these measurements was 50 mV and 50 ms, respectively. The peak potential, E_p vs Pt pseudoreference, for dopamine, norepinephrine, and 5-HT were found to be 0.087, 0.0957, and 0.1719 V, respectively. During these measurements and other measurements using cyclic voltammetry on pristine nanofiber electrodes, oxidation of 5-HT was noted to passivate the nanofiber electrode, putatively due to the formation of nonconductive films at overoxidizing potentials. This is consistent with other studies where phenolic and hydroxyindole oxidation products arising from serotonin have been documented to form insoluble, passivating films on the surface of electrodes during in vivo brain measurements.[18]

Cell Attachment and Differentiation on Nanofiber Electrode Arrays. The attachment and differentiation of both the derived Rat pheochromocytoma cell line (PC-12) and dissociated rat hippocampal cells were both investigated in this study. PC-12 cells have often been used in studies of neuronal development due to their ability to differentiate into more neuronal-like morphologies upon the addition of exogenous proteins, such as nerve growth factor[19,20] Under proliferative culture conditions (high serum with no exogenously added nerve growth factor, NGF), PC-12 cells exhibit a rounded morphology with cell bodies measuring approximately 10−15 μm in diameter. These cells tend to clump and proliferate in multilayer foci, with little to no generation of processes. In the absence of NGF, earlier studies of this cell line reported that PC-12 cells were electrically inexcitable. Differentiation in NGF, however, increases the density of Na channels in the membrane, thereby increasing the cell's excitable behavior.[21] NGF also induces dramatic changes in cellular morphology. In the presence of low serum and NGF, individual cells cease proliferation and rapidly begin to generate neurite outgrowths. Initiation of processes begins within 24 h of NGF addition and extension continues over a period of weeks. Localized swollen regions, or varicosities, can often be observed along these neurite outgrowths and particularly at the junction of neurites from separate cells. Studies with single-element, carbon-based microelectrodes have demonstrated that both differentiated and nondifferentiated PC-12 cells can be induced, via either electrical stimulus or application of chemical secretogogues, to exocytose catecholamine neurotransmitters, specifically dopamine. By placing beveled carbon electrodes at different locations upon both differentiated and undifferentiated PC-12 cells, Zerby and Ewing demonstrated that dopamine can be exocytosed from the cell body of undifferentiated cells, but becomes localized largely to varicosities of neurite processes following NGF-induced differentiation.[22]

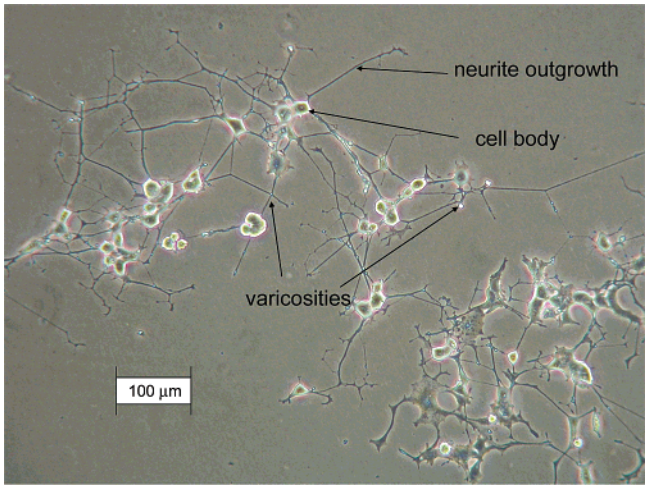

Figure 2. Phase contrast micrograph of PC-12 cells in Nunc-Delta plates following 14 days of differentiation in nerve growth factor. Neurite outgrowth from the cell body often resulted in varicosities at neurite junctions.

Figure 2 presents a phase contrast micrograph of PC-12 cells after 14 days of differentiation on commercially available Nuncdelta plates (Nunclon, Roskilde, Denmark) in low serum/NGF media. In this image, neurite outgrowth can clearly be distinguished from the more rounded bodies of individual PC-12 cells. Often, varicosities can be observed at the junction of these processes. Figure 3 presents similar micrographs of PC-12 differentiation after 12 days in NGF media on a Type I and a Type II nanofiber array. Again, neurite outgrowths can be distinguished, typically in regions that are sparsely populated with cells. In our system, the surface of the nanofiber array is coated with a passivation layer of the UV-cross-linked epoxy, SU-8. Without specific treatment, SU-8 normally presents a hydrophobic surface that discourages wetting as well as cellular attachment. Treatment with oxygen plasma, however, can be used to increase the hydrophilicity and the surface roughness of the SU-8, and cellular attachment can readily be achieved

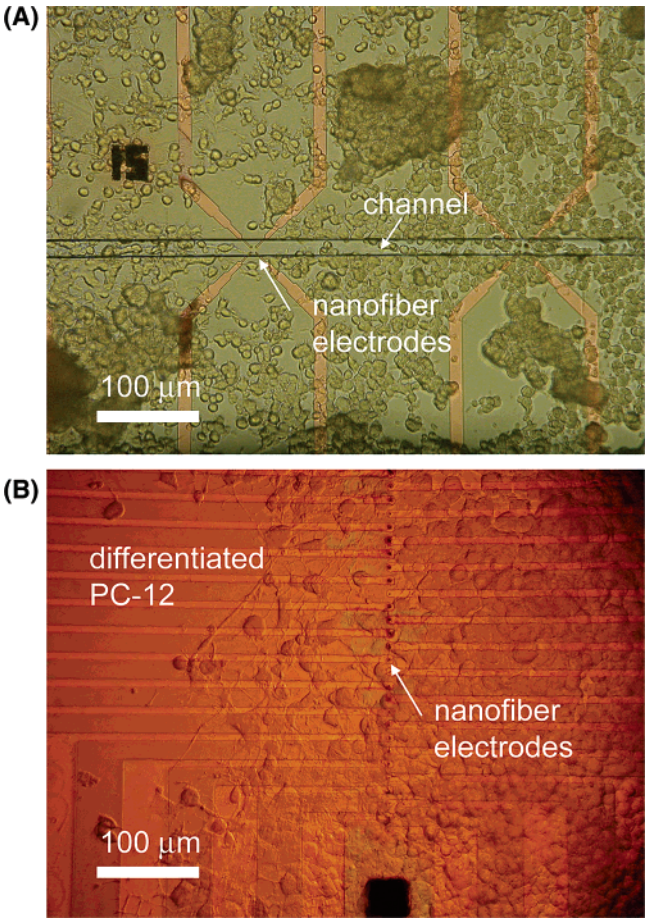

Figure 3. Reflection optical micrograph of PC-12 cells cultured in differentiation media for 12 days on the oxygen-plasma treated SU-8 surface of a Type I (A) and Type II (B) nanofiber array. While this imaging mode does not provide the same level of detail as phase contrast, neurite outgrowth and varicosities can be distinguished in the nonconfluent regions of the culture. Nanofiber electrodes are seen as black dots at the termini of each interconnect.

with a variety of cell types. In this study, electrode chips were individually treated prior to device packaging with a 30 s rf plasma in a Trion Oracle etcher using 50 sccm oxygen, 150 W rf power, and at a pressure of 150 mTorr. This treatment was noted to significantly roughen the SU-8 surface and increase its hydrophilicity, as noted by coarse wetting contact angle observations. Following this treatment, cells could be cultured directly onto the surface with no further treatment, or specific coatings such as soaking in solutions of fibronectin or poly-L-lysine could be employed to putatively enhance attachment and neurite outgrowth. In this study, significant differences in the initial attachment and subsequent neurite outgrowth were not observed between untreated SU-8 surfaces and those treated with PLL. However, often after a period of 7−10 days and with handling, cells cultured on the untreated SU-8 surface would become unattached. This loss of adhesion was typically rapid and complete across the entire cell matrix, likely due to the loss of a small patch of cells and the subsequent shear imparted to the remaining cell layer due to its connectivity with the released regions. In contrast, arrays treated with 50 μg/mL of PLL did not experience this complete unattachment phenomenon but did experience some detachment at small, local regions of cells. Interestingly, arrays treated with similar dilutions of fibronectin generally displayed very poor cell adhesion.

The opacity of the substrate of both Type I and Type II nanofiber arrays caused some interference with optical imaging of neurite outgrowth. Typically, phase contrast imaging is used to examine cellular features during imaging of biological structures. This mode of imaging, however, requires transmission through the sample, which is not possible with the opaque, silicon-based substrate of our devices. Therefore, parts a and b of Figure 3 were obtained using a semiconductor inspection microscope (Mitutoyo, AF1) which operates in a reflective mode without phase contrast. As such, there is considerable loss of contrast in this image and in the ability to resolve individual neurite outgrowths. To observe these processes in more detail, some samples were fixed and imaged with SEM. Parts a, b, and c of Figure 4 present scanning electron micrographs of day-16 (parts a and b of Figure 4) and day 7 (Figure 4c) differentiated PC-12 cells. Cells were first fixed in 2% gluteraldehyde in PBS solution and methanol dehydrated then imaged at low acceleration voltages (1 kV) without further modification. Neurite extensions can clearly be resolved, as can varicosities along the neurite length. These neurite outgrowths appear to extend in arbitrary directions with respect to the nanofiber electrode array but could occasionally be found to run along the line of a nanofiber array, as seen in Figure 4b. The presence of a nanofiber in the path of an extending neurite also appears to occasionally redirect the outgrowth (Figure 4c). It is anticipated that future efforts to pattern nanofiber arrays, or to pattern extracellular matrix materials around nanofiber arrays, may be used to promote such patterned extension of neurite outgrowth[23,24] However, these studies were not included in this effort. Rather, cell attachment and neurite extension were allowed to occur without specific chemical or electrical cues from the array substrate. As such, electrode/neurite placement was not directed. We relied upon microscopic inspection and the large number of available electrodes in order to find specific individual electrodes that were well positioned for electrophysiological study in regions adjacent to cells.

Electroanalytical Measurement of Adherent Neuronal Cultures. Following typically at least six days of differentiation in culture of PC-12 and dissociated rat hippocampal cells, electroanalysis was performed at individual nanofiber electrodes. Cultured arrays were aspirated of media, rinsed in Tyrodes, placed under Tyrodes solution at 37 °C, and then inspected in a reflection-based semiconductor inspection scope to identify specific electrodes that may be well positioned with respect to a differentiated region of cells (such as presented in Figure 3 above). The cultured array was then transferred to an electroanalytical workstation comprised of a heated faraday cage and a potentiostat. A platinum pseudoreference electrode was flame sterilized and placed in the Tyrodes solution with care so as to not mechanically interact with the cell layer upon the nanofiber array electrodes. Measurement at individual electrodes, including both fixed potential amperometry and moderate scan cyclic voltammetry (0.5−10 V/s sweep rates) was then conducted via computer control through the potentiostat.

For both Type I and Type II arrays, it was noted that the first sweep of many electrodes positioned in regions with high numbers of PC-12 cells often exhibited a significant oxidation wave on the first sweep that did not reoccur during immediately subsequent sweeps but would reoccur if the culture was allowed to rest in Tyrodes solution without probing for approximately 1 h. Figure 5a presents the first, second, and third sweeps on a Type II electrode cultured with PC-12, six differentiation days in vitro (DIV). A significant oxidation wave is observed on the first sweep, peaking at 0.5 V, but this wave does not reoccur

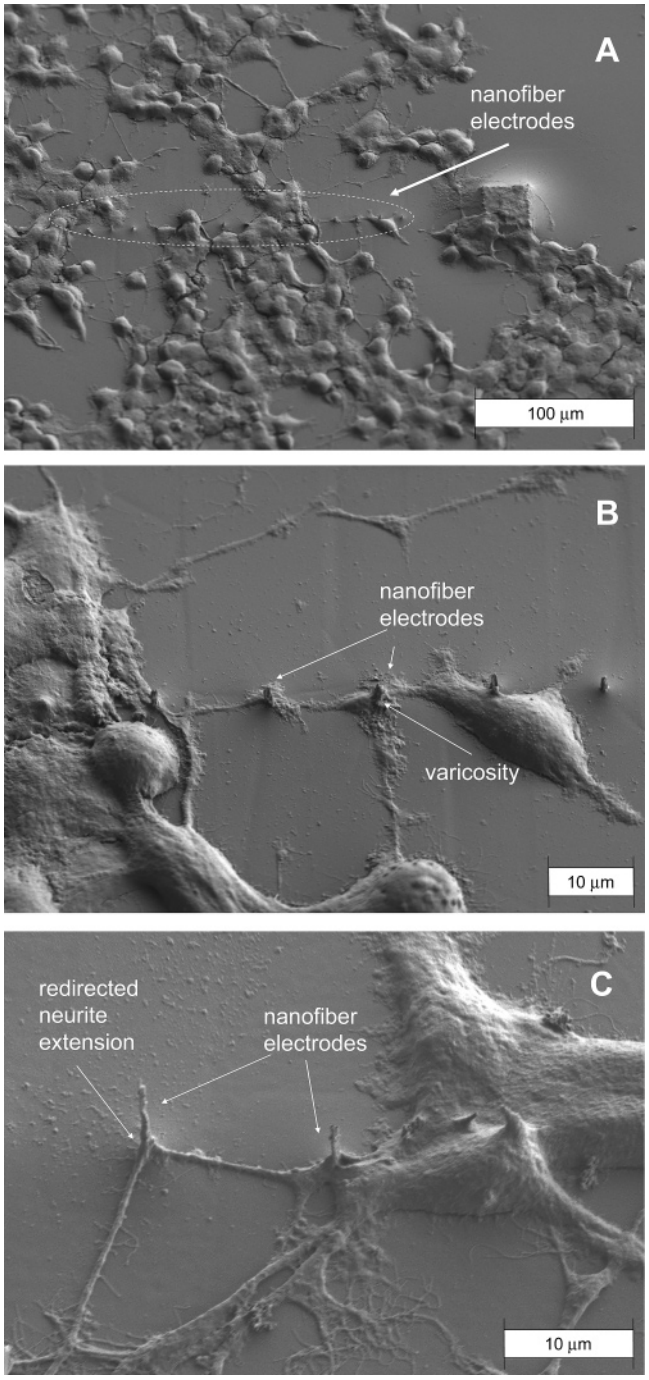

Figure 4. Scanning electron micrographs of differentiated PC-12 cells on a Type II nanofiber array. Prior to imaging, cells were fixed in 2% gluteraldehyde and dehydrated with methanol. (A) The neurite processes of differentiated PC-12 cells can clearly be distinguished as can occasional varicosities at neurite junctions. (B) A putative varicosity is located in close proximity to an individually addressed nanofiber electrode. (C) Occasionally, neurite extensions appear redirected due to interaction with nanofiber electrodes.

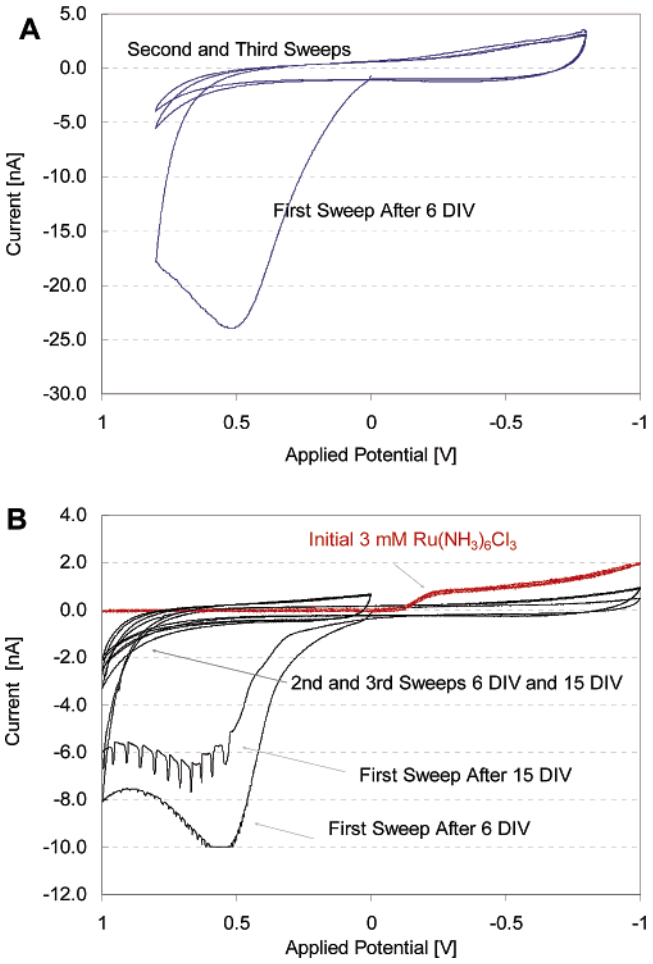

Figure 5. (A) Initial voltammetric sweep following long-term culture and differentiation (6 DIV) of PC-12 cells on a Type II array. The initial sweep shows a large oxidative peak, putatively due to the accumulation of easily oxidized material(s) on or around the electrode. Subsequent sweeps do not indicate this large oxidative response, putatively due to analyte burnoff. (B) Occasionally during this initial oxidative wave, oxidative transients are observed, shown here at DIV 6 and 15 of PC-12 on a Type I array as compared against the initial preculture characterization trace with 3 mM $Ru(NH_3)_6Cl_3$.

during subsequent sweeps. We anticipate that this oxidative wave corresponds to burnoff of an easily oxidized species either upon or around the nanofiber electrode. SEM has indicated that nanofibers can often be located beneath the body of a cell, or group of cells. For example, in Figure 4b, the position of the leftmost nanofiber in the image can be seen as a bump in the body of the overlaying cell. Confocal and electron microscopy has also indicated (data not shown) that such positioning may form a pocket beneath the cell, where the nanofiber serves much like a tent pole in supporting a sequestered volume beneath the overlaying cell. This volume could accumulate electroactive species over time. The response of an electrode in such a restricted volume would be one much like that described by Clark and Ewing, where single-element carbon fiber microelectrodes were used to probe small, micromachined volumes (390 pL) containing limited amounts of analyte or a small number of excitable cells.[25,26] At appropriately slow scan rates, all of the material within such a confined volume is oxidized (or reduced) resulting in a response very similar to the initial anodic wave presented in Figure 5a. In Clark and Ewing's picoliter vials, 6−10 bovine adrenal cells within a 390 pL volume produced such a response that was interpreted in their study as being easily oxidized catecholamines generated by the resident cells (estimated to be approximately 60 μM of, for example, norepinephrine or epinephrine). In our system, a restricted volume may be generated due to the configuration of the cell membrane being supported by the nanofiber electrode. Application of oxidizing potentials to such a volume would result in a similar exhaustive analyte oxidation wave during both voltammetry and amperometry. Such a response may also be seen to some extent if the nanofiber electrode is sequestered in an invagination of the cell membrane. Again, within such an invagination, easily oxidized species could be accumulated in

the closed volume during culture and exhaustively oxidized during the initial sweep of the voltammogram, or during the initial periods of amperometry. This initial oxidation wave may also be due in part to the oxidation of species that have accumulated onto the electrode, rather than in the volume around the probe, during long-term cell culture. In either case, however, the wave was dependent upon the continued presence of adjacent cells. The initial oxidative wave could be regenerated after approximately 1 h of no activity on the electrode. Removal of cells by agitating the surrounding solution with a pipet resulted in loss of the ability to regenerate this signal.

Occasionally during this first large oxidative response and more infrequently during subsequent sweeps, spiking of the voltammetric trace was observed at potentials greater than approximately 0.4 V. For example, Figure 5b presents the first, second, and third sweeps following both 6 DIV and 15 DIV of PC-12 culture on a Type I array. The first sweep of each demonstrates the large oxidative wave but also features numerous individual oxidative spikes superimposed upon the large oxidative wave. For the 15 DIV trace, these spikes are very pronounced, ranging from 10 to 15 ms in duration and 1−5 pC in oxidized charge. This spiking behavior was only observed at electrodes that were located in close proximity to cells and, like the larger oxidative wave, was eliminated upon removal of the cells.

While apparently dependent on the presence of cells, this spiking activity could be due to several mechanisms. First, it could be a physical/mechanical phenomenon associated with cellular response to the applied cyclic waveform and associated charge effects. For example, deformation of the electrode or dielectric layers may result in transient changes in electrode surface area, such as at the dielectric/electrode interface. The spiking activity may also be associated with excitable responses of the cells, and associated membrane depolarizations. Extracellular carbon-based electrodes have frequently been used for electrophysiological recording from excitable cells and tissue, where charge coupling to the electrode results in current/voltage spiking activity at the electrode during evoked or spontaneous membrane depolarization.[2] As such, spiking activity could be due to such coupling with spontaneous excitable activity or evoked membrane depolarization resulting from the applied waveform at the electrode and/or analyte burnoff. Typically, however, extracellular voltage spikes due to membrane depolarization are of shorter duration (<10 ms) and are bi- or triphasic, whereas the spikes indicated in Figure 5b are monophasically oxidative. Following the excitatory stimulus, they would also tend to be independent of the applied voltage on the electrode rather than found, as in our case, only at oxidizing potentials greater than approximately 0.4 V.

Another potential explanation for these spikes that would account for their presence only above 0.4 V is exocytosis and oxidation upon the nanofiber electrode of vesicles of easily oxidized catecholamines, such as dopamine or norepinephrine. Against a platinum pseudoreference in Tyrodes solution, dopamine, norepinephrine, and serotonin can be oxidized on carbon nanofibers at 0.087, 0.0957, and 0.1719 V, respectively. Previous studies referenced throughout this manuscript have demonstrated that both amperometry and fast scan cyclic voltammetry (FSCV) can be used to observe individual exocytotic events from a variety of excitable cell types, including PC-12. In amperometry, the electrode is poised at a potential sufficient to oxidize the species of interest. In FSCV, the electrode is cycled rapidly (typically at 100+ V/s) through a range of potentials that can both oxidize the initial species as well as to potentially reduce the generated oxidized product. In either of these methods, oxidative spikes result from the impingement of easily oxidized materials upon the surface of the electrode. During exocytosis, these spikes are quantal in nature, due to the release of these materials in vesicular quanta. Integration of the current under each spike during either amperometry or voltammetry[6] provides measurement of the charge oxidized (or reduced) during each transient event and therefore quantitation of the number of species oxidized via the relationship

$$N = Q/nF$$

Here, N is the number of moles oxidized, Q is the amount of charge from each current transient, n is the number of electrons transferred for each oxidized molecule (2 for catecholamines), and F is Faraday's constant (96485 C/equiv). For the current spikes of Figure 5b, the charge under each spike would correspond to putative vesicular contents of approximately 5−25 attomoles, or approximately 3 000 000−15 000 000 putative catecholamine molecules. These values are reasonable with respect to documented vesicular quanta in other excitable cell types, but rather high for PC-12. For example, Finnegan et al. amperometrically studied the vesicular content of a variety of cell types using a conventional carbon electrode placed temporarily in contact with the cell membrane.[27] In their study, the vesicular content was reported as histograms of the cube root of the charge of the current transient of individual exocytotic events. By use of the expression above and the reported mean values for the cube root of the charge for each cell type, human pancreatic β cells were found to have a mean vesicular content of ∼600 000 molecules, bovine chromaffin cells had a mean content of ∼2 100 000 molecules, and rat mast cells had a mean content of ∼3 700 000. Rat pheochromocytoma was found in their study to have a mean vesicular content of only ∼125 000 molecules. Our putative oxidative spikes for PC-12 are considerably larger. Nonetheless, it has been documented that PC-12 can exhibit significant plasticity in vesicular quantal size. Sombers et al. employed L-3,4-dihydroxyphenylalanine and reserpine to increase and decrease, respectively, the volume of single pheochromocytoma cell vesicles, with resulting vesicular size ranging from 1×10^4 to 3.2×10^6 molecules (or the equivalent of ∼1 fC−1 pC in oxidized charge during each current transient).[28] The individual quanta of Figure 4b are still approximately 10× the maximum values reported by Sombers for vesicular size in PC-12.

Figure 6 presents the response of dissociated embryonic rat hippocampal cells after 16 DIV during cyclic voltammetry at an individual nanofiber electrode of the Type I device. As with PC-12 cells, putative oxidative bursts can be discriminated after the first set of sweeps (a and b) at potentials greater than 0.4 V on each of the subsequent 3 sweeps (c, d, and e). In this case, however, no initial oxidative wave induced the spiking activity. Further, spiking activity was seen not on the first sweep, but rather on subsequent sweeps and only at sufficiently oxidizating potentials (>0.4 V) to oxidize, for example serotonin or norepinephrine. At lower potentials, spiking activity was either not occurring, or was occurring but could not be detected due to the electrode being poised at unsufficient oxidizing potentials. Evaluating individual spikes ($n = 10$), the duration of discrete spikes averages approximately 8.9 ± 2.1 ms with individual spikes ranging from approximately 0.1 to 0.17 pC. This charge under each spike would correspond to vesicular contents of approximately 0.50−0.90 attomoles, or approximately 300 000−550 000 putative catecholamine molecules. Also apparent is the

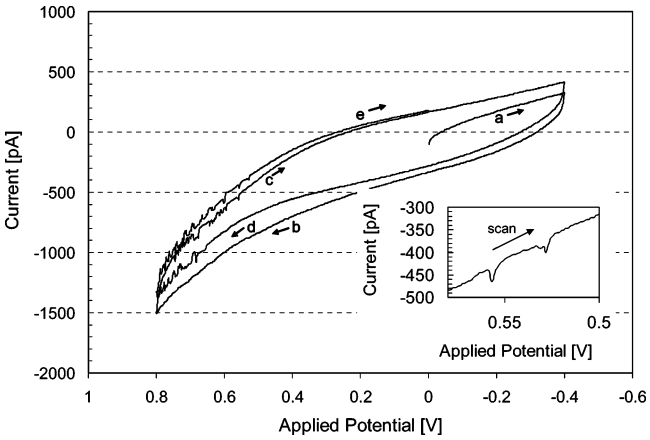

Figure 6. Cyclic voltammogram of response of a Type I array following 16 days of culture and differentiation of E18 cells (scan rate 1 V/s, Pt pseudoreference). Oxidative bursts can be distinguished as pulses in sweeps c, d, and e of the voltammogram. These spikes only occur at potentials greater than 0.4 V, sufficient potential for the oxidation of dopamine and norepinephrine.

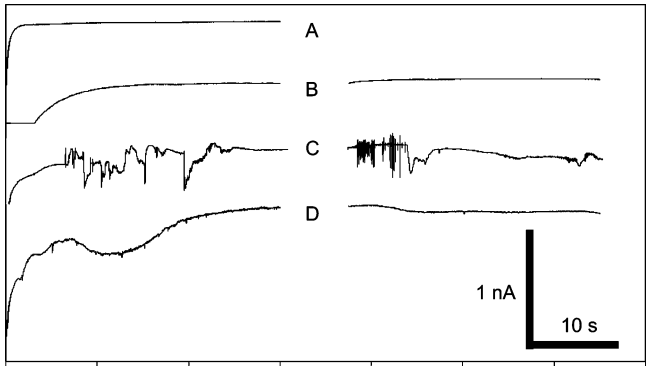

Figure 7. Amperometric traces (800 mV vs Ag|AgCl) recorded from a Type I array with and without undifferentiated PC-12 cells. Trace A: cell free trace. Trace B: confluent layer of undifferentiated PC-12 cells upon application of Tyrodes solution. Trace C: cell response to application of Tyrodes with 1 mM nicotine. Note that spiking activity begins at approximately 7 s and continues through subsequent 30 s traces. Trace D: following several minutes in the nicotine solution, cells were rebathed in Tyrodes without nicotine. Some occasional spiking activity continued for several minutes. Note, each trace was conducted for 30 s. Breakage of the traces from $t = 30-37$ s represents a lost data period due to rerunning the amperometric trace.

presence of a *foot* preceding some oxidative spikes (inset). This preceding foot has been well documented in the literature, and may correspond to the fusion of individual vesicles with the cell membrane and leakage of material from a fusion pore prior to full exocytosis.[6,28] In the inset of Figure 6, the second oxidative peak of the trace exhibits a preceding foot approximately $^1/_2$ of the height of the total oxidative transient.

It should be noted that dopaminergic cells are not expected to be found in dissociated cultures of embryonic rat hippocampi nor do these cells typically produce vesicles of any easily oxidized neurotransmitter. In contrast, GABA/glutamate are the predominant neurotransmitters of these regions, and neither of these were found to be electroactive at the indicated potentials on our unmodified carbon nanofiber electrodes (data not shown). As such, it is surprising to see spiking activity putatively from easily oxidized neurotransmitters, such as dopamine, norepinephrine, and serotonin. Cells from the hippocampal region of the brain are typically *stimulated* by afferent dopaminergic cells, but are not themselves dopaminergic. Nonetheless, expression studies have determined that infrequently rat hippocampal cells do indeed express at high levels the mRNAs for tyrosine hydroxylase, DOPA decarboxylase, and dopamine hydroxylase (i.e., the enzymes responsible for dopamine and norepinephrine generation from their precursor, tyrosine).[29,30] There may therefore be mechanisms where dissociated cells from this tissue could differentiate down a dopaminergic path, perhaps to compensate for unavailability of dopaminergic afferents in the dissociated culture.

The responses indicated in Figures 5 and 6 were not frequently observed at nanofiber electrodes, only typically being seen at a few electrodes of a 40-element array during any one probing period. During the test run captured in Figure 6, responses were seen at 2 other electrodes of 10 total probes that were identified to be in close proximity to cells. In contrast to the response of Figure 6, however, these electrodes captured a series of extended (∼100 ms) oxidative events that could not be resolved into individual, discrete spikes. Such response would be consistent with an electrode placed at a larger distance from the site of exocytosis than the electrode of Figure 6. Greater distance from the point source would result in diffusion of the exocytosed material in the cell/electrode gap and arrival of overall less material over a longer period of time, and perhaps from multiple sources, at the electrode surface. As such, the oxidation spikes due to exocytosis of individual vesicles would not be as clearly defined as individual events as those at a closer spaced electrode. Readers interested in additional detail of the spatially dependent responses of such electrodes are referred to Anderson et al.[31]

We anticipated that the infrequency of capturing these dynamic events was likely associated with low cell densities and low probability of having ideal cell/electrode coupling. In these experiments, low cell seeding densities were used to promote neurite differentiation. With PC-12, differentiation is inhibited by closely spaced cells and thus low seeding densities are used. Further, vesicular release in PC-12 is known to be restricted almost entirely to varicosities following differentiation.[22] With dissociated rat hippocampal cells, there is also the fact that few, if any, dopaminergic or norepinephrinergic cells are generated during the differentiation process.[29] All of these factors make it very improbable for a fixed location nanofiber electrode to be situated appropriately to be capable of observing the exocytotic event.

Further, in each of the responses during these test runs, and in other tests of both dissociated rat hippocampal and PC-12 cells, spiking activity would sometimes be seen on the first set of scans (3 full cycles from 0 to −0.5 to 0.8 V and back to 0 V), and occasionally the second, but could not be reestablished during that same measurement period after the first set of scans. Subsequent attempts to re-evaluate these spikes using the more conventional approach of constant potential amperometry were conducted but typically resulted in no detectable activity or large, apparently oxidative, bursts that were far too large to be accredited to individual vesicular events. Application of a secretogogue (100 mM K+) could infrequently induce a similar large response from these same electrodes, but these responses could not be discriminated definitively from the noise associated with the delivery itself.

To overcome these limitations, Type I arrays were seeded with very high numbers of nondifferentiated PC-12 cells such that electrode/cell proximity could be ensured. Following overnight culture, the growth media was exchanged with three washes with 37 °C Tyrodes solution. The arrays were then visually inspected to verify that a confluent layer of cells remained present on the electrodes. Amperometric (800 mV vs Ag|AgCl) and voltammetric measurements (−0.5 to 1.0 V

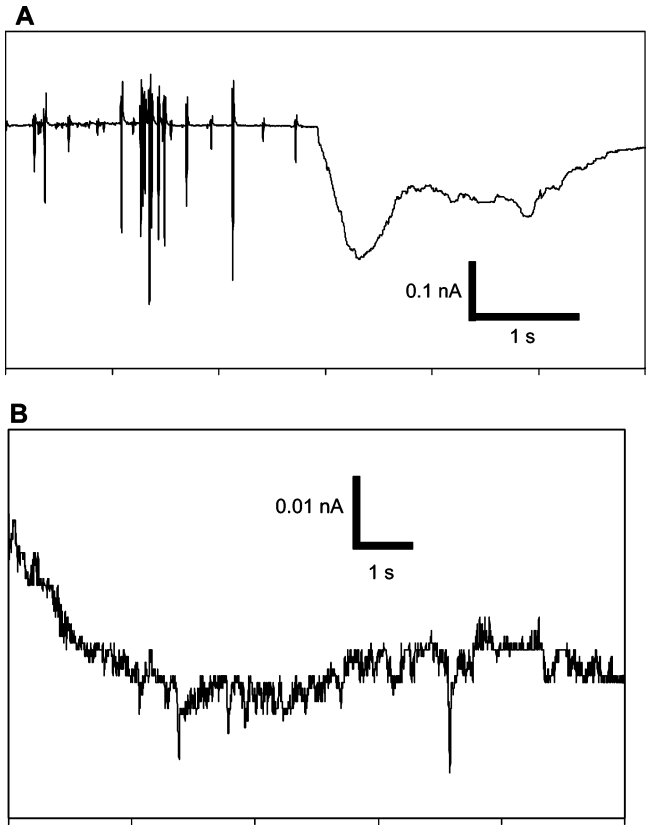

Figure 8. (A) Detail of amperometric trace from Figure 7c, from 41 to 47 s. Spikes associated with extracellular voltage transients are observed and appear to result in release of large amounts of easily oxidized material, at approximately $t = 44$ s. (B) Following replacement with Tyrodes, individual oxidative spiking activity is observed for several minutes following the stimulus.

sweeps at 1 V/s) were then performed in media, Tyrodes solution, and in Tyrodes solution with nicotine added as a secretogogue (1 mM). In media and Tyrodes, no dynamic spiking events similar to those of Figures 5 and 6 were observed. Replacement of the fluid volume with fresh Tyrodes solution also generated no spiking activity. A representative trace following such replacement is provided in Figure 7b. Nicotine was then applied as a secretogogue to induce membrane depolarization and exocytosis of the confluent cell layer. Nicotine has been established as a secretogogue with a significant period of latency (15−30 s) between its application and subsequent membrane depolarization.[32] Following the full volume replacement with a 37 °C solution of 1 mM nicotine in Tyrodes, dramatic spiking activity commenced, with a representative trace provided in Figure 7c. During the first 30 s of this amperometric trace, significant activity began approximately 15 s following the application of the nicotine solution, consistent with an expected latency period as documented by Zerby and Ewing. This spike activity continued for approximately 120 s and included both rapid pulse trains of biphasic spikes as well as cumulative increases and dramatic shifts in the oxidative current (Figure 7c). Pulse train activity was exhausted within approximately 2 min, but individual discrete spikes that were monophasically oxidative continued to occur over a period of 4 min on multiple electrodes of an array. Replacement with Tyrodes solution and repetition of the nicotine challenge, however, resulted in no additional spiking activity (Figure 7d). Following the experiment, removal of the cell layer via mechanical dissociation and reiteration of the experiment resulted in no spiking activity, thereby eliminating the potential of device failure, such as wiring or dielectric breakdown, potentially resulting in spike behavior (Figure 7a).

Inspection of the spikes and current shifts of Figure 7c demonstrates classic voltage spiking behavior observed with extracellular carbon electrodes upon membrane depolarization, as well as apparent resultant shifts in oxidative current. These shifts are putatively due to the massive release of easily oxidized species from the large number of depolarized cells. Magnified portions of trace 7c are presented in Figure 8. In contrast to earlier experiments with sparse populations of differentiated cells, crowding of the cells in these experiments resulted in large numbers of both types of responses, i.e., spikes associated with extracellular voltage transients in addition to abrupt changes in oxidative current. While spikes associated with individual extracellular voltage transients could clearly be observed (Figure 8a), the ability to also see individual exocytotic events was likely confounded by the massive release of easily oxidized material simultaneously from a large number of cells. Nonetheless, individual oxidative spikes could be discerned during the late periods of this evoked response and for several minutes after replacement of the solution with Tyrodes without nicotine (Figure 8b). We anticipate that future efforts at patterning both cell seeding and their subsequent differentiation will enable us to optimize the spatial arrangement of nanofiber electrodes with active regions of differentiated cells, thereby promoting the ability to capture and record discrete dynamic events associated with neuronal communication.

Conclusions

This study has established that arrays of nonplanar, high aspect ratio nanofiber electrodes may be employed as growth substrates for relatively long-term culture and differentiation (at least 16+ days) of neuronal cells. Nanofibers are electrochemically active structures that may be integrated into parallel arrays using the conventional tools and approaches of microfabrication. Similar to planar electrode arrays, nanofiber electrodes may be employed in a *resident* interfacing mode, where neuronal cells are cultured, differentiated, and electroanalytically evaluated *directly* on the electrode array. In contrast to conventional planar arrays, however, nanofibers provide a novel, nonplanar, high aspect ratio structure that may provide unique opportunities for probing extra-, inter-, and ultimately intracellular phenomena. In this study, we have provided preliminary data that indicates such resident nanofibers may be employed for electroanalytical studies of neuronal cells. We anticipate that future efforts with patterning neuronal differentiation upon nanofiber arrays and temporal electrophysiological probing of the differentiating cultures will provide unique insights into neurogenesis, neuropharmacological response, and the fundamental mechanisms and subtleties of cell to cell signaling via synaptic transmission.

Acknowledgment. The authors wish to thank P. H. Fleming and T. Subich for assistance with metal depositions and D. Thomas for assistance with photolithography. This work was supported in part by the National Institute for Biomedical Imaging and Bioengineering under Assignment 1-R01EB000433-01, by the Material Sciences and Engineering Division Program of the Department of Energy Office of Science under Contract DE-AC05-00OR22725 with UT−Battelle, LLC, and through the Laboratory Directed Research and Development funding program of the Oak Ridge National Laboratory, which is managed for the U.S. Department of Energy by UT−Battelle, LLC. A portion of this research was conducted at the Center

for Nanophase Materials Sciences, which is sponsored at Oak Ridge National Laboratory by the Division of Scientific User Facilities, U.S. Department of Energy.

References and Notes

(1) Kissinger, P. T.; Hart, J. B.; Adams, R. N. *Brain Res*. **1973**, *55*, 209−213.

(2) Armstrong, J. M.; Millar, J. *J. Neurosci. Meth*. **1979**, *1*, 279−287.

(3) Wightman, R. M.; Jankowski, J. A.; Kennedy, R. T.; Kawagoe, K. T.; Schroeder, T. J.; Leszczyszyn D. J.; Near, J. A.; Diliberto, F. J. Jr.; Viveros, 0. *Proc. Natl. Acad. Sci. U.S.A.* **1991**, *88*, 10754−10758.

(4) Anderson, B. B.; Ewing, A. G. *J. Pharm. Biomed. Anal.* **1999a**, *19*, 15−32.

(5) Hochstetler, S. E.; Puopolo, M.; Gustincich, S.; Raviola, E.; Wightman, R. M. *Anal. Chem.* **2000**, *72*, 489−496.

(6) Troyer, K. P.; Wightman, R. M. *J. Biol. Chem.* **2002**, *277*, 29101−29107.

(7) Wightman, R. M.; Haynes, C. L. *Nat. Neurosci.* **2004**, *7*, 321−322.

(8) Daws, L. C.; Toney, G. M.; Davis, D. J.; Gerhardt, G. A.; Frazer, A. *J. Neurosci. Meth.* **1997**, *78*, 139−150.

(9) Zhou, F.-M.; Liang, Y.; Salas, R.; Zhang, L.; De Biasi, M.; Dani, J. A. *Neuron* **2005**, *46*, 65−74.

(10) Guillorn, M. A.; McKnight, T. E.; Melechko, A. V.; Austin D. W.; Merkulov, V. I.; Simpson, M. L.; Lowndes, D. H. *J. Appl. Phys.* **2002**, *91*, 3824−3828.

(11) McKnight, T. E.; Melechko, A. V.; Austin, D. W.; Sims, G. T.; Guillorn, M. A.; Simpson, M. L. *J. Phys. Chem. B* **2004**, *108*, 7115−7125.

(12) McKnight, T. E.; Melechko, A. V.; Griffin, G. D.; Guillorn, M. A.; Merkulov, V. I.; Serna, F.; Hensley, D. K.; Doktycz, M. J.; Lowndes, D. H.; Simpson, M. L. *Nanotechnology* **2003**, *14*, 551−556.

(13) Merkulov, V. I.; Lowndes, D. H.; Wei, Y. Y.; Eres, G.; Voelkl, E. *Appl. Phys. Lett*. **2000**, *76*, 3555−3557.

(14) Merkulov, V. I.; Hensley, D. K.; Melechko, A. V.; Guillorn, M. A.; Lowndes, D. H.; Simpson, M. L. *J. Phys. Chem. B* **2002a**, *106*, 10570−10577.

(15) Merkulov, V. I.; Melechko, A. V.; Guillorn, M. A.; Lowndes, D. H.; Simpson, M. L.; Whealton, J. H.; Raridon, R. J. *Appl. Phys. Letts*. **2002b**, *80*, 4816−4818.

(16) Merkulov, V. I.; Melechko, A. V.; Guillorn, M. A.; Lowndes, D. H.; Simpson, M. L. *Appl. Phys. Lett.* **2002c**, *80*, 476−478.

(17) Melechko, A. V.; McKnight, T. E.; Hensley, D. K.; Guillorn, M. A.; Borisevich, A. Y.; Merkulov, V. I.; Lowndes, D. H.; Simpson, M. L. *Nanotechnology* **2003**, *14*, 1029−1035.

(18) Stamford, J. A.; Justice, J. B., Jr. *Anal. Chem.* **1996**, *68*, A359-A363.

(19) Greene, L. A.; Tischler, A. S. *Proc. Natl. Acad. Sci. U.S.A.* **1976**, *73*, 2424−2428.

(20) Dichter, M. A.; Tischler, A. S.; Greene, L. A. *Nature*, **1977**, *268*, 501−504.

(21) Rudy, B.; Kirschenbaum, B.; Rukenstein, A.; Greene, L. A. *J. Neurosci.* **1987**, *7*, 1613−1625.

(22) Zerby, S. E.; Ewing, A. G. *Brain Res.* **1996**, *712*, 1−10.

(23) Branch, D. W.; Wheeler, B. C.; Brewer, G. J.; Leckband, D. E. *IEEE Trans. Biomed. Eng.* **2000**, *37*, 290−300.

(24) Nam Y.; Chang J.; Khatami, D.; Brewer, G. J.; Wheeler, B. C. *IEEE Proc. Nanobiotechnol.* **2004**, *151*, 109.

(25) Clark, R. A.; Ewing, A. G. *Anal. Chem*. **1998**, *70*, 1119−1125.

(26) Clark, R. A.; Ewing, A. G. *Chemtech* **1998**, *28*, 20−25.

(27) Finnegan, J. M.; Pihel, K.; Cahill, P. S.; Huang, L.; Zerby, S. E.; Ewing, A. G.; Kennedy, R. T.; Wightman, R. M. *J. Neurochem.* **1996**, *66*, 1914−1923.

(28) Sombers, L. A.; Hanchar, H. J.; Colliver, T. L.; Wittenberg, N.; Cans, A.; Arbault, S.; Amatore, C.; Ewing, A. G. *J. Neurosci.* **2004**, *24*, 303−309.

(29) Aubert, M.; Guiramand, J.; Croce, A.; Roch, G.; Szafarczyk, A.; Vignes M. *Cerebral Cortex* **2001**, *11*, 878−887.

(30) Datson, N. A.; van der Perk, J.; de Kloet, E. R.; Vreugdenhil, E. *Hippocampus* **2001**, *11*, 430−444.

(31) Anderson, B. B.; Zerby, S. E.; Ewing, A. G. *J. Neurosci. Meth.* **1999**, *88*, 163−170.

(32) Zerby, S. E.; Ewing, A. G. *J. Neurochem*. **1996**, *66*, 651−657.